JOURNAL OF GEOPHYSICAL RESEARCH, VOL. 102, NO. A2, PAGES 2093–2103, FEBRUARY 1, 1997

Motion and erosion of the nightside plasmapause region and of the associated subauroral electron temperature enhancement: Cosmos 900 observations

V. V. Afonin and V. S. Bassolo
Space Research Institute, Moscow, Russia

J. Smilauer
Institute of Atmospheric Physics, Prague, Czech Republic

J. F. Lemaire
Institut d'Aéronomie Spatiale de Belgique, Bruxelles, Belgium

Abstract. Ion densities N_i and electron temperatures T_e measured on board Cosmos 900 satellite (launched at March 30, 1977, into near-polar circular orbit: $i = 83°$, $h = 500$ km, orbital period = 94 min) are used to study the behavior of the ionosphere during the prestorm, initial, and main phases of the magnetic storm of December 1–2, 1977. The spatial resolution of the measurement was $\leq 0.3°$ latitude for T_e and $\leq 0.1°$ latitude for N_i. During this period, 27 orbits were recorded in the onboard large-storage memory. This enabled detailed study of the positions and latitude profiles of midlatitude ionospheric trough and subauroral electron temperature enhancement (SETE) in the midnight local time sector. Simultaneous proton density data measured on the high-altitude satellites "Prognoz 5" and "Prognoz 6" confirm that the poleward boundary of the T_e peak corresponds to the ionospheric magnetic field projection of the high-altitude plasmapause density "knee." During the main phase of a geomagnetic storm the polar edge of the SETE becomes very steep. It coincides with an equally steep poleward edge of the midlatitude ionospheric trough and with the position of the newly forming density gradient of the high-altitude plasmapause. The sequence of Cosmos 900 observations clearly shows how the nighttime midlatitude ionospheric trough fills up as well as how the subauroral electron temperature enhancement and the outer layers of the plasmasphere are eroded during a geomagnetic storm. These results shed new light on the formation of the plasmapause in the postmidnight sector and on the time-dependent electric field distribution in the nightside sector before and during a geomagnetic storm.

1. Introduction

More than 2 decades ago, *Muldrew* [1965], *Thomas and Andrews* [1968], *Rycroft and Thomas* [1970], *Rycroft and Burnell* [1970], and *Tulunay and Sayers* [1971] found midlatitude ionospheric troughs (MIT) in the electron density N_e at F region altitudes and above. They attempted to relate these MIT to the high-altitude plasmapause as determined by *Gringauz* [1961] from the Soviet Lunik observations and by early whistler measurements of *Carpenter* [1966] and others.

The correlation has been reasonably good on the nightside where the MIT is most clearly identified. Indeed, statistically, the invariant latitude of this trough varies with K_p in a manner quite similar to the equatorial plasmapause density gradient. However, in the subsequent years, until 1986, this interpretation had been questioned since at times, and especially in the afternoon-dusk sector, the magnetic field lines corresponding to the high-altitude plasmapause are located poleward of the ionospheric MIT in most cases when this feature could be identified [*Grebowsky et al.*, 1976, 1978; *Titheridge*, 1976; *Foster et al.*, 1978].

On the other hand, using ISIS 1 observations, *Brace and Theis* [1974] noted a distinct peak in the electron temperature T_e located within the steep N_e gradient of the middle-latitude plasmapause on the nightside. They suggested that this subauroral electron temperature enhancement (SETE) corresponds to the field-aligned projection of the high-altitude plasmapause (PP) and that this temperature peak which is clearly identifiable at all local times down to at least 600 km altitude might be used to trace the movements of the plasmapause under variable geomagnetic conditions. However, they noted that the magnetic local time (MLT) distribution of the SETE did not exhibit the bulge in the dusk sector that is characteristic of the equatorial plasmapause as measured by whistler propagation [*Carpenter*, 1970] and by in situ satellite measurements [*Chappell et al.*, 1971; *Taylor et al.*, 1970].

The midlatitude peak in T_e was not a new feature. *Brace and Reddy* [1965] and *Brace et al.* [1967] reported it as a nighttime phenomenon, already observed a decade earlier with an electrostatic probe on board of Explorer 22 at an altitude of 1000 km. Other independent thermospheric electron temperatures measurements by a Langmuir probe on the polar-orbiting sat-

Paper number 96JA02497.
0148-0227/97/96JA-02497$09.00

ellite ESRO 1 made before, during, and after a geomagnetic storm, between October 31 and November 1, 1968, clearly confirmed the existence of a peak in the latitudinal electron temperature profiles in the subauroral region. This midlatitude peak was observed at conjugated points in both hemispheres, in the altitude range 280–1500 km, and has been associated by *Raitt* [1974] with stable auroral red arcs (SAR arcs) observed in the midnight local time sector. The position of this electron temperature peak shifted to lower invariant latitude when K_p increased during the main phase of the geomagnetic storm. It moved slowly back to higher latitude during the recovery phase when K_p decreased. This equatorward and poleward shift of the SETE temperature peak was found to be very similar to the inward and outward motion of the equatorial plasmapause position, as observed by whistlers, and to the position of SAR arcs. Similar results were reported by *Brace et al.* [1974] based on ISIS 2 polar satellite measurements (at 1400 km altitude). They traced the latitudinal shifts of the midlatitude electron and ion temperatures peaks during the magnetic storm of August 4–6, 1972, with a time resolution of 2 hours universal time (UT), corresponding to the orbital period of ISIS 2. The occurrence frequency of well-identified SETEs versus altitude was studied by *Büchner et al.* [1983] based on observations of Intercosmos 18. They found that the occurrence frequency between 400 and 800 km depends more strongly on altitude in the dayside local time (LT) sector than in the nightside one.

Although these low-altitude observations tended to indicate an association between the SAR arcs, the midlatitude electron temperature peak, and the midlatitude ionospheric trough, the question remained as to how the subauroral electron temperature peak observed on average at an invariant latitude of 60° ($L \sim 4$) was really related to the location of the equatorial plasmapause. The answer to this question came more than a decade later from coordinated measurements of DE 2 and DE 1 satellites launched in August 1981. DE 1 traversed the plasmapause at altitudes of the order of 10,000 km, while DE 2 crossed the plasmapause L shells at altitudes below 1000 km. *Green et al.* [1986] and *Horwitz et al.* [1986] found that the subauroral electron temperature enhancement in the 1900–2000 LT sector occurs on field lines which thread the equatorward edge of a steep density gradient, which is located inside the plasmasphere closer to the Earth than the "whistler knee," at least in this MLT sector. To distinguish both steep plasma density gradients, the former has been called the "inner plasmapause," while the latter is called the "outer plasmapause." The inner plasmapause has an almost circular MLT distribution unlike the outer plasmapause which may have a bulge in the afternoon-dusk sector. *Brace et al.* [1988] showed that this sharp internal gradient in plasmaspheric H^+ density marks the field lines of the F region T_e ledge, that is, that both features are physically associated and statistically lie on the same L shells, near $L = 4$ at magnetically quiet times.

Therefore most of the contradicting results were based on observations in the afternoon local time where it is now recognized that there are multiple plasmapause knees in the equatorial density profiles [see *Carpenter et al.*, 1993]. At night when, according to the classification of *Horwitz et al.* [1986], featureless plasmapause are observed most of the time the correspondence between the MIT and equatorial plasmapause is most obvious.

In section 2 we examine simultaneous high time resolution measurements from the low-altitude Cosmos 900 satellite on polar orbit and from the high-altitude Prognoz 5 and 6 satellites, to confirm the close association between the subauroral electron temperature enhancement (SETE) and the high-altitude PP. In section 3 we describe how the profile and location of the SETE changes in the postmidnight sector during a large geomagnetic storm event. As a result of their high time resolution these Cosmos 900 observations shed new light on the sequence of events during the erosion of the nightside plasmasphere. They also unravel earlier views on the penetration of magnetospheric convection electric fields in the nightside plasmasphere.

2. Physical Association Between MIT, SETE, and the PP Ion Density Gradient

2.1. Description of the Observations and Spacecraft Orbits

Cosmos 900 was launched on March 30, 1977, on a near-polar orbit with inclination of 83°, altitude of 500 km, and orbital period of 1.5 hours. It operated for more than 2.5 years. During this time, span Prognoz 5 and 6 were operating on high-altitude orbits with inclination of 65° and apogees of about 200,000 km altitudes. Prognoz 5 and 6 made plasma measurements at high altitudes over a wide range of invariant latitudes up to ±65° ($L \sim 5.6$), like those of DE 1 which was launched 4 years later.

Cosmos 900 provided plasma observations in 1977 in the topside ionosphere, along an orbit similar to the DE 2 satellite, which was launched in 1981. The instrumentation on board of Cosmos 900 was designed to measure the electron temperature (T_e) and the ion density (N_i). The temperature T_e was measured by the method of RF electron temperature probe, which is known as "rectification probe" and described by *Afonin et al.* [1973]. This method was originally proposed by *Aono et al.* [1961]. The N_i was determined both by planar and spherical retarding potential analyzers (RPA). The time resolution of T_e measurements was quite high: 4 s. The spherical RPA operated in "floating mode" of the outer grid so that the time resolution for N_i measurements was equal to the telemetry rate, that is, 1 s in the 1-day storage memory mode. Hence the spatial resolution was better than 0.3° and 0.1° in latitude, respectively, for T_e and N_i (i.e., 36 and 12 km, respectively). Thus these high time resolution data are suitable to study ionospheric features such as the midlatitude ionospheric trough and the subauroral electron temperature enhancement.

Note that the time resolution and consequently the spatial resolution of Cosmos 900 electron temperature measurements were more than a factor of 3 higher than those of the ESRO 1 measurements of 1968 reported by *Raitt* [1974] and 30 times better than the ISIS 1 and 2 electron temperature observations of 1972 reported by *Brace and Theis* [1974] and *Brace et al.* [1974]. The electron temperature measurements of 1981 made by DE 2 [*Brace et al.*, 1988] had a spatial resolution of 40 km which was comparable to Cosmos 900 (36 km). Therefore Cosmos 900 enabled to resolve for the first time in 1977 the extremely steep temperature gradient sometimes observed at the poleward edge of SETEs.

The RPA on board of Prognoz 5 and 6 are described in the work of *Gringauz et al.* [1981] and *Gringauz* [1983]. The high-altitude measurements of the ion density (N_i) and ion temperature (T_i) have been obtained with a time resolution of 80 s.

2.2. Quiet Time Observations

During the periods of time considered below, the high- and low-altitude satellites traversed the plasmapause and MIT/

SETE regions in the same local time sector. Figure 1 shows the relevant parts of the orbits of Cosmos 900 and Prognoz 5 in L, MLT coordinates on April 13, 1977, which was a quiet day with Kp values of 2+, 0+, 2−, 1, 1+, 1+, 1, and 2.

It can be seen that the orbit segments of both spacecraft are close to each other in the 2200–2400 MLT sector. Cosmos 900 traversed the magnetic shell $L = 4$ at 0257 UT and again 1.5 hours later at 0430 UT at an altitude of 510 km. The crossings of this magnetic shell by Cosmos 900 occur almost 2 hours in local time later than that of Prognoz 5.

The ion densities and electron temperatures measured during these two consecutive traversals of the MIT are shown in Figure 2 as a function of L along Cosmos 900 orbits 217 (solid lines) and 218 (dashed lines), respectively. These measurements were made during quiet conditions (K_p = O+) along Cosmos 900 orbits 217 and 218.

The Prognoz 5 ion density and ion temperature also shown in Figure 2 are measured at high altitudes between 8200 and 14,000 km. The altitudes of Prognoz 5 are given by the lower scale; the corresponding L is also given. Prognoz 5 traversed the magnetic shell $L = 4$ at 0354 UT, that is, 1 hour after Cosmos 900 did traverse this shell during orbit 217 and almost a half an hour before it did so again during orbit 218.

It can be seen that under these quiet conditions the subauroral electron temperature enhancements have nearly symmetrical slopes on both sides of the T_e peak. Note also that the SETE is consistently located at the outer edge of the ion density gradient forming the equatorward boundary of the MIT. These results agree with those obtained by *Brace and Theis* [1974] using ISIS 1 Langmuir probe measurements at altitudes between 600 and 3000 km.

From the dotted line (N_i) in Figure 2 it can also be seen that the steep ion density gradient observed above 10,000 km altitude by Prognoz 5 is located at $L = 4.8$, that is, precisely between the L shells where the SETE was observed by Cosmos 900, respectively, 1 hour earlier ($L = 4.3$) and a half an hour later ($L = 5$). This is consistent with an outward motion of the nightside plasmapause at a rate of 0.5 R_E/h and a simultaneous poleward motion of the SETE under quiet conditions or when K_p is decreasing. This outward motion of the nightside plasmapause during quiet conditions is supporting the existence of a continuous, slow expansion of the plasmasphere [*Lemaire and Schunk*, 1994].

Prognoz 5 was located in a local time sector more than 1 hour MLT closer to the duskside region than Cosmos 900. Therefore one may argue that the universal time variations of the three plasmapause crossings is biased by a possible local time variation of the position of the plasmapause. However, this is not likely to be the case according to the observations of *Carpenter and Anderson* [1992]. Indeed, their ISEE measurements indicate that the equatorial plasmapause is closely circular in this LT sector, at least in a statistical sense.

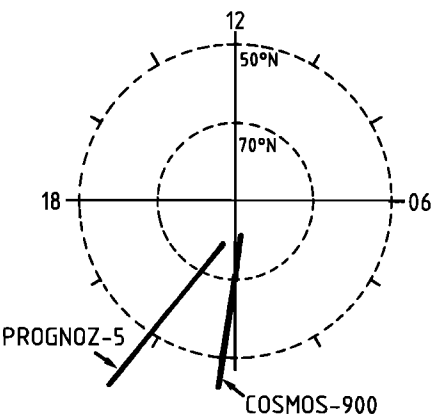

Figure 1. Projections of three orbits of Cosmos 900 on a magnetic local time (MLT) versus invariant latitude map in the northern hemisphere.

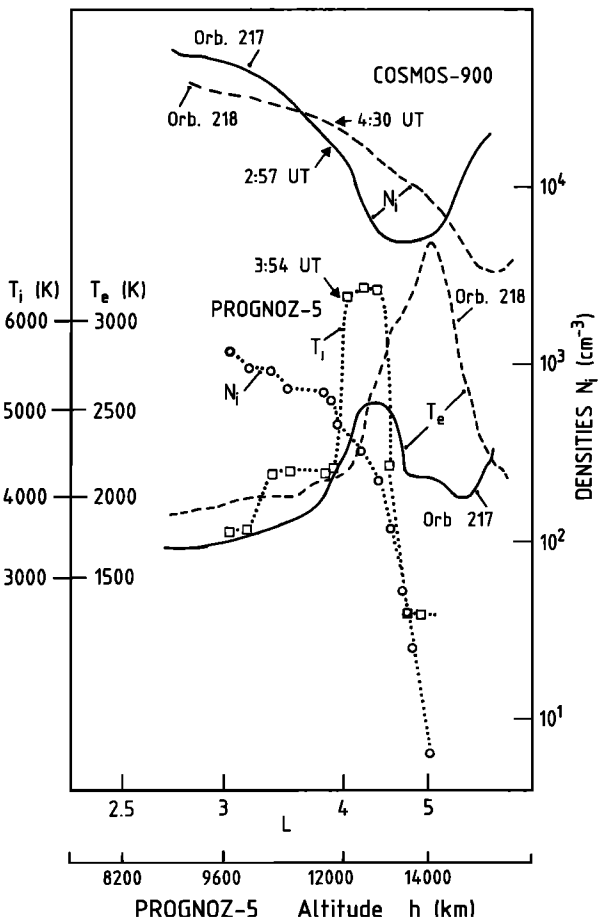

Figure 2. Low-altitude ion densities (N_i) and electron temperatures (T_e) observed on April 13, 1977, along two consecutive orbits of Cosmos 900 as a function of L. The dotted lines with open symbols give the ion density and ion temperature (T_i) measured almost simultaneously at high altitude in the same MLT sector along Prognoz 5 orbit. The altitude of Prognoz 5 is shown on the scale at the bottom of the figure. These data correspond to quiet geomagnetic conditions.

The correspondence between the positions of SETE and of the high-altitude plasmapause is consistent with DE 1/DE 2 observations, indicating that both features are indeed related to each other and physically connected [*Green et al.*, 1986; *Kozyra et al.*, 1986, 1987; *Brace et al.*, 1988]. *Horwitz et al.* [1986] found evidence in the DE 2 measurements that the T_e enhancement in the F region occurs on field lines which map into the plasmasphere or plasmapause region at a point where the density is about 10^3 cm^{-3}.

The dotted lines (T_i) in Figure 2 give the ion temperature measured by Prognoz 5 at high altitude. It can be seen that the value of T_i increases in the outer region of the plasmasphere, which has been called the "hot zone" by *Gringauz and Bezrukikh* [1976].

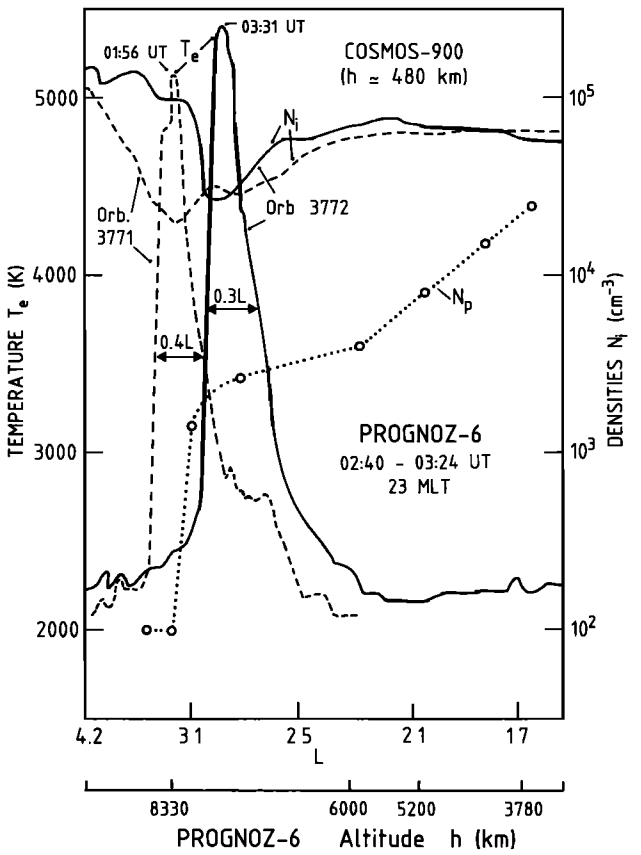

Figure 3. Low-altitude ion densities and electron temperatures observed on December 2, 1977, along two consecutive orbits of Cosmos 900 as a function of L. The dotted line with open circles gives the ion density (N_i) measured almost simultaneously in the same MLT sector along Prognoz 6 orbit at high altitude (see altitude scale at the bottom of the figure). These data sets are obtained during a period of increasing geomagnetic activity. Note the equatorward shift of the subauroral electron temperature enhancement (SETE) when *Kp* increases.

This enhancement of the high-altitude ion temperature in the vicinity of the plasmapause is generally attributed to wave particle interactions. There are many papers dealing with this suggestion. However, other plasma kinetic effects have also been proposed, for example, the velocity filtration effect leading to positive ion temperature gradients in the outermost layer of the plasmasphere when the velocity distribution functions of the ions have an enhanced non-Maxwellian tail [*Pierrard and Lemaire*, 1996]. It is not the scope of this paper to discuss these heating mechanisms of the outer plasmasphere.

Since the peak of the high-altitude ion temperature is located at a different (lower) L than the peaks of the low-altitude SETE, we are tempted to conclude that both features are not on the same set of magnetic field lines and therefore are not directly related to each other, that is, the SETE is not a direct consequence of field-aligned heat transferred from the high-altitude hot ions to the ionospheric electrons. As already indicated above, we do not consider that the 1-hour difference in MLT of the Cosmos 900 and Prognoz 5 is likely to explain such an offset in the L values of both temperature peaks.

2.3. Simultaneous Observations at High and Low Altitudes During Disturbed Conditions

In the previous section we discussed simultaneous high- and low-altitude data obtained during quieting geomagnetic conditions. Figure 3 illustrates observations obtained during disturbed conditions on December 2, 1977 (see the *Kp* and *Dst* indexes for this period of time in Figure 5a).

The high-altitude measurements of N_i were collected between 0240 and 0324 UT with Prognoz 6 in the altitude range 3700–8400 km in the 23 MLT sector and for L ranging between 1.7 and 4.2. The high-altitude plasmapause density gradient is observed at $L = 3.1$.

Corresponding Cosmos 900 data (T_e and N_i) were collected at a lower altitude (480 km) in the 5–6 MLT sector. The solid and dashed lines in Figure 3 show the density and temperature profiles obtained respectively along two consecutive orbits (3771 and 3772) of Cosmos 900 when it moved from high latitudes to low latitudes across the MIT. The SETE was traversed at $L = 3.2$ (0156 UT) and at $L = 2.9$ (0331 UT). The MLT and invariant latitudes of the relevant portion of Cosmos 900 orbits 3764–3773 are shown in Figure 4.

Note that the T_e peaks have a much steeper poleward edge than in Figure 2. One might again consider that this is due to the variation of steepness of the electron temperature profile with local time, since the Cosmos 900 measurements shown in Figure 2 were obtained near-midnight MLT, while those of Figure 3 refer to the dawn local time sector. However, in the light of *Carpenter and Anderson* [1992], observations indicating that the steepness of the equatorial plasmapause is an increasing function of MLT, such an explanation does not hold. The most likely explanation is therefore that the midnight temperature profiles of Figure 2 were obtained during much quieter geomagnetic conditions than the steeper ones observed near dawn and shown in Figure 3. These conclusions are confirmed by the results shown below in Figure 6.

It is the sharp poleward edge of the SETE that has been used by *Brace et al.* [1988] in their statistical analysis of DE 2 to identify the location of the "inner plasmapause projection" at ionospheric heights. This characteristic signature of SETE can be identified in Cosmos 900 and DE 2 observations with an accuracy of a few tenths of a degree in latitude. Note that the maximum of T_e is usually located at a lower L value than this sharp poleward edge of the SETE. Note also that the slope of the equatorward wing of the SETE is not significantly steeper

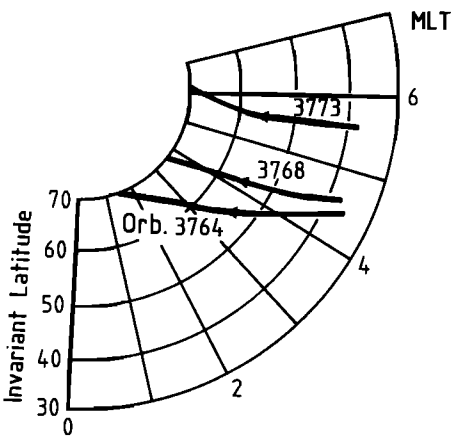

Figure 4. Projection of three orbits of Cosmos 900 in the MLT versus invariant latitude map.

during disturbed conditions than it was during quiet times, as shown in Figure 2. Of course, this is not the case for its poleward wing. The extreme sharpness of the poleward edge could not be resolved by the earlier Explorer 22, ISIS 1 and 2, and ESRO 1 probes because of their lower time/spatial resolutions.

The steep plasmapause density gradient in the high-altitude ion density was observed at 0250 UT when Prognoz 6 traversed the shell $L = 3.1$. The near simultaneity in UT as well as the near coincidence in L of the plasmapause and SETE again confirm that there is a close physical relation between both features, even during disturbed geomagnetic conditions. This conclusion is based on the assumption that the shape of the plasmapause is nearly circular (i.e., independent on MLT) in the postmidnight sector. According to *Carpenter and Anderson*'s [1992] statistical study of the plasmapause positions, this is a reasonable assumption.

Between orbits 3771 and 3772, *Kp* has increased from 5 to 7−. As a consequence of this enhanced geomagnetic activity, the nightside plasmapause is expected to form at smaller L, that is, closer to Earth [*Chappell et al.*, 1970], and the SETE is therefore expected to shift closer to the equator, as shown in Figure 3.

The magnitude of the electron temperature peak increases with increasing values of the magnetic activity index *Dst*. This was already mentioned by *Büchner et al.* [1983] and by *Kozyra et al.* [1986]. It can be verified from Figure 3 that the width of the SETE at half peak value shrank from $0.4L$ to $0.3L$ during its equatorward shift between the two consecutive orbits of Cosmos 900. This observation confirms again that the width of the SETE (at half peak height) is more narrow during disturbed conditions than during very quiet times. The reduction of this width is also consistent with the decrease of thickness of the equatorial plasmapause region when *Kp* increases [*Chappell et al.*, 1970].

Having set the stage by describing in this first part the format of the Cosmos 900 observations and having also confirmed with independent data sets that the SETE is a reliable low-altitude signature of the nightside equatorial plasmapause, we will now describe in detail the evolution of the position and shape of the SETE during the development of a geomagnetic storm. A number of statistical studies of the SETE locations and maximum peak temperatures have been published (see references already quoted above), but so far event studies of the SETE during a geomagnetic storm have not yet been published with spatial and time resolutions as high as those of Cosmos 900. Section 3 of this article aims to fill in this gap.

3. Evolution of the Subauroral Electron Temperature Enhancement During a Geomagnetic Storm

The data (N_i and T_e) presented below were collected along a set of consecutive orbits of Cosmos 900 (from orbit 3748 to 3776) including the period of the geomagnetic storm of December 1–2, 1977. The invariant latitudes and magnetic local times along three of these orbits are shown in Figure 4. The data displayed in Figure 6 are all collected in the postmidnight local time sector. Figure 5a shows the values of the *Kp* and *Dst* magnetic indexes during the time of observation. Before the geomagnetic storm started, *Kp* has been smaller than 2− for more than 12 consecutive hours.

At 1500 UT December 1, Cosmos 900 is on its orbit 3764. The ion density and electron temperature measured during this orbit, under quiet (prestorm) conditions, are shown as reference profiles in Figure 6 by light solid lines. On the following orbit (3765), geomagnetic conditions are still quiet. This profile will correspond here to time $t = 0$, that is, the beginning of the geomagnetic storm.

The density and temperature profiles shown by heavy solid lines in Figure 6a are almost the same as during the preceeding reference orbit (3764). The equatorward wing of the density trough did not change and has an exponentially decreasing slope. The subauroral electron temperature enhancement extends over 10° invariant latitude with a maximum T_e value of 5000–6000 K at 58°–62°. Small-scale structures are present on the poleward side of the temperature peak.

It can also be seen that the poleward side of the ion density trough has an extremely steep gradient forming a "wall" or ledge on the equatorward side of the auroral region. In the time period of 1.5 hours, between orbit 3764 and 3765, this wall has shifted equatorward from 64° to 63° invariant latitude. This shift is a result of the slight increase of geomagnetic activity: indeed, *Kp* has increased from 1− to 2− during that period of time (see Figure 5a).

An additional increase of *Kp* to a value of 3+ occurred during the following orbits (3766 and 3767) of Cosmos 900, respectively, at $t = 1.5$ and 3 hours. The result is an additional shift of the sharp auroral density wall down to 60° invariant latitude as can be seen in Figures 6b and 6c. It can also be seen in these panels that the poleward wing of the subauroral electron temperature enhancement has changed from a rather irregular slope of about 1000 K/degree latitude to a steep negative gradient larger than 40,000 K/degree latitude. This ledge in the temperature profile is precisely located at the same latitude as the positive density wall: the ledge of the SETE moves equatorward with the same speed as the auroral density wall. However, so far the equatorward wing of the temperature enhancement remains unchanged during this initial period of time. Only the poleward wing of the SETE is modified as a result of the equatorward propagation of the auroral ionization density front.

The trend outlined above continues during the following orbits of Cosmos 900 for 12 hours since (i.e., until orbit 3773 shown in Figure 6h), while *Kp* increased progressively up to a maximum value of 7− on December 2, 1977, between 0300 and 0600 UT. By that time, *Dst* has reached its minimum value and the density wall has reached an invariant latitude as low as 51° ($L \cong 2.52$). However, note that it is only 3 or 4 hours after the beginning of the storm that the wing of the temperature profile equatorward of the peak starts moving southward (see Figure 6d corresponding to orbit 3768 at $t = 4.5$ hours). It is important to emphasize that during the first 3 or 4 hours the invariant latitude of the temperature peak did not change. The temperature and density distributions on the equatorward wing of the SETE did not change either during these first 3 or 4 hours after the onset of the geomagnetic storm.

The existence of SETEs with extremely sharp poleward edges was also found in the observations of DE 2, which had a time resolution similar to those of Cosmos 900 [*Brace et al.*, 1988]. However, as emphasized above, during very quiet conditions this sharp ledge is absent and becomes a rather irregular temperature profile as shown in Figure 6a. The irregular small-scale structures of T_e are attributed to irregular magnetospheric particle precipitation patterns.

The solid dots in Figure 5b indicate the positions (L) of the subauroral electron temperature enhancement well before the

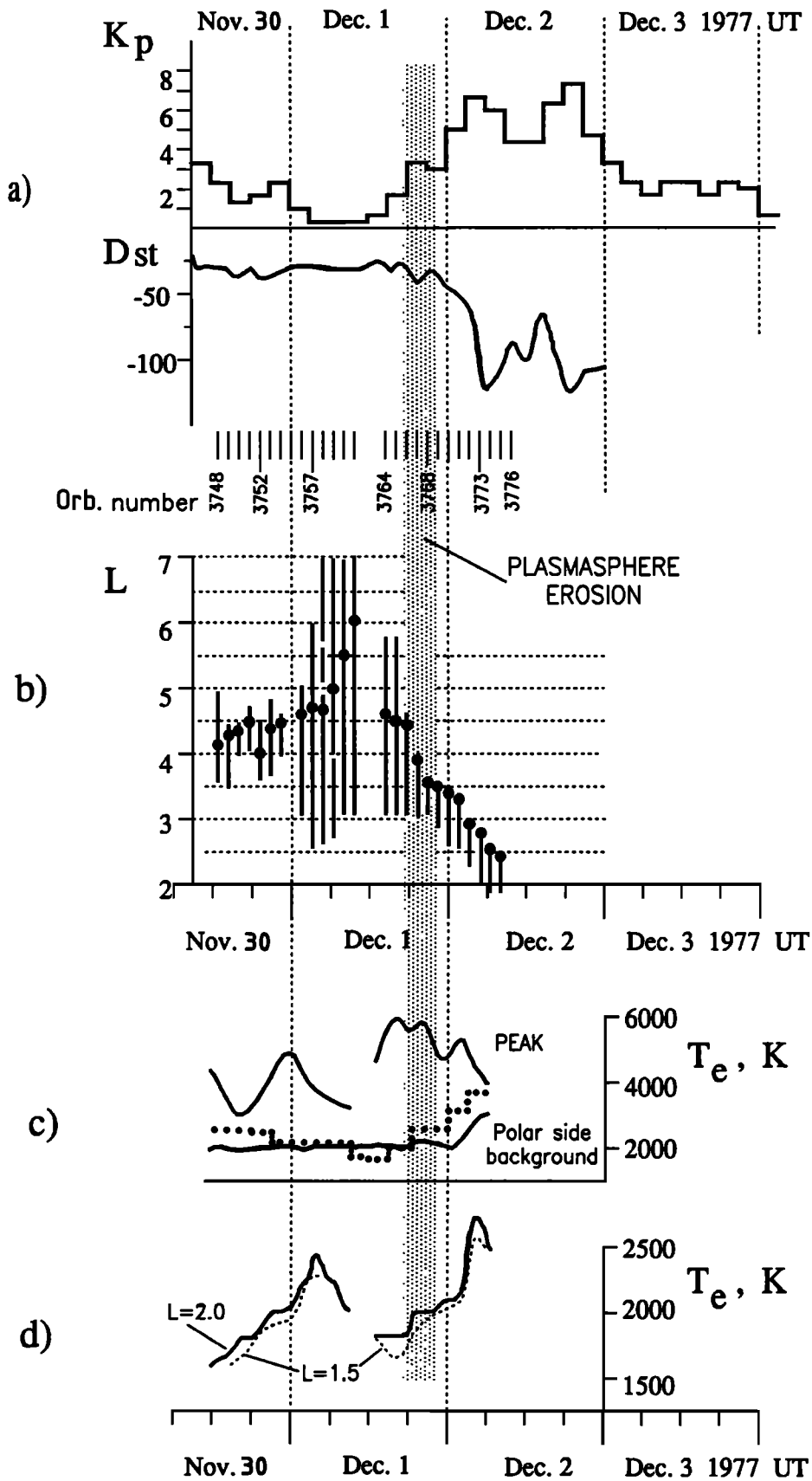
a)
Kp
Nov. 30
Dec. 1
Dec. 2
Dec. 3 1977 UT
8
6
4
2
Dst
-50
-100
Orb. number
3748
3752
3757
3764
3768
3773
3776
b)
L
7
6
5
4
3
2
PLASMASPHERE
EROSION
Nov. 30
Dec. 1
Dec. 2
Dec. 3 1977 UT
c)
PEAK
Polar side
background
6000
4000
2000
Te, K
d)
L=2.0
L=1.5
2500
2000
1500
Te, K
Nov. 30
Dec. 1
Dec. 2
Dec. 3 1977 UT

geomagnetic storm commencement (orbit 3748), up to orbit 3776, after the main phase. The vertical line segments correspond to the latitudinal extent of the SETE. During November 30 and early December 1, the position of the equatorial plasmapause (as identified by the SETE in the ionosphere) moves to higher L, while Kp decreased during this period of time. This is in agreement with the relationship

$$L_{pp} = 5.6 - 0.46\ Kp_{max} \quad (1)$$

where Kp_{max} is the maximum Kp value in the preceding 24 hours. This relation was first proposed by *Carpenter and Park* [1973] and recently confirmed by *Carpenter and Anderson* [1992].

From their statistical study based on DE 2 observations, *Brace et al.* [1988] found similar relationships depending on the value of Kp' which is a modified Kp index defined as the following: Kp' is the highest 3-hour Kp value which occurred during the 12-hour period preceding the measurements. This magnetic parameter was also adopted by *Kozyra et al.* [1986] because it provided the best ordering of the T_e signatures. The use of Kp_{max} or Kp' rather than the 3-hour Kp recognizes that the expansion of the plasmapause following substorm activity is slow because the refilling process has a time constant of several days.

Brace et al. [1988] found that the locations of the T_e maximum at nightside fit the linear relation

$$L' = 6.06 - 0.6\ Kp' \quad (2)$$

This relation was deduced from DE 2 data during solar maximum conditions (i.e., in 1981). From AE-C measurements during solar minimum (1976–1977), *Brace* [1990] finds a different relation for the nightside SETE location

$$L'' = 5.40 - 0.34\ Kp' \quad (3)$$

Figure 7 shows the values of L', L'', and L_{pp} predicted by (1), (2), and (3). These predictions are compared to the T_e peak positions (dots) observed by Cosmos 900 which were obtained during solar minimum conditions. It can be seen that the relationship of *Brace et al.* [1988] approximately fits the Cosmos 900 observations. However, as already shown in Figure 6, it is only 3 hours after the storm commencement that the position of the T_e maximum begins to shift to more innerward magnetic shells. This time lag of 3 hours can hardly be appreciated in Figure 7 since the time resolution of Kp_{max} and Kp' indexes is equal to 3 hours. However, this time lag is clearly evident in Figure 6.

In other words, the location of plasmapause as derived from the position of the SETE in the postmidnight sector does not shift to lower L values immediately after the onset of a geomagnetic storm or substorm. It takes a certain lapse of time (3–4 hours) before the erosion or peeling of the nightside plasmasphere takes place at lower magnetic shells. This delay corresponds to the time which is needed for the auroral ionization front to drift from high invariant latitudes (>65°) across the midlatitude ionospheric trough.

F region signatures, including zonal ion velocities associated with dc electric fields in a different (dusk) sector, have shown a similar time delay of 3–6 hours for a geoelectric disturbance to propagate from high latitude to lower latitudes [*Miller et al.*, 1990].

4. Interpretation of the Results and Discussion

4.1. Nonuniform Enhancement of the Electric Field

Our results indicate that the erosion of the plasmasphere takes place in the postmidnight local time sector, when and where the equatorward edge of the auroral region is shifting closer to the equator and reaching magnetic field lines corresponding to the location of the quiet time SETE maximum. At high altitude in the magnetosphere this should be associated with the sunward motion of a cloud of plasmasheet particles. If this interpretation is correct, the convection electric field within this plasma cloud must have an enhanced westward component. The existence of a westward E field is supported by the observed equatorward shift of the auroral ionization front shown in Figure 6.

Equatorward to this propagating ionization front the latitudinal distribution of the ionospheric plasma density is unperturbed during the first 3 or 4 hours following the beginning of the geomagnetic strom in the early phase of the storm. This implies that the convection velocity is unchanged there. This implies also that the convection electric field (as measured in a frame of reference corotating with the Earth) has a nearly zero-westward component on the equatorward side of the propagating ionization wall, while this westward E field component is nonzero on its poleward side. In other words, during the inital phase of a magnetic storm, the convection electric field distribution may correspond to that of a finger-like plasma cloud intruding into an almost unperturbed plasmatrough and eventually into the nightside plasmasphere. This tentative interpretation needs to be checked with future global imaging missions to the magnetosphere.

At a fixed instant of time the westward electric field component is not enhanced at all magnetic shells, contrary to what is currently assumed in Kp-dependent convection electric field models, like for instance the shielded Volland-Stern models [*Volland*, 1973, 1975, 1978; *Stern*, 1977]. Indeed, in these electric field models the dawn-dusk component of the E field is assumed to change in phase with Kp simultaneously at all locations in the magnetosphere. The results illustrated in Figure 6 indicate that this was not the case on December 1, 1977: the time-dependent convection electric field associated with the magnetic storm was not a uniformly distributed enhancement of the dawn-dusk component. The effects of the inward propagating electric field enhancement were observed first on the more distant magnetic shells and only later on those closer to Earth.

Figure 5. (Opposite) (a) Values of the geomagnetic indexes Kp and Dst for a series of days in November and December 1977, including a large geomagnetic storm. The times corresponding to the relevant portions of orbits of Cosmos 900 are given by the orbit numbers from 3748 to 3776. (b) Values of L corresponding to the peak electron temperature (solid dots) and width at half of the peak height (vertical bars) of the SETE as measured by long successive orbits of Cosmos 900 at low altitude (480 km) in the northern hemisphere in the postmidnight MLT sector. (c) Values of the peak electron temperature measured in the SETE by Cosmos 900. The temperature in the auroral region poleward of the midlatitude ionospheric trough is also shown. (d) Values of the effective temperature of the electrons at $L = 2$ (solid line) and $L = 1.5$ (dashed line) on the equatorward side of the SETE. These effective temperature measurements are obtained from the determination of the slope of current-voltage characteristics over an interval centered around the floating potential of the spacecraft.

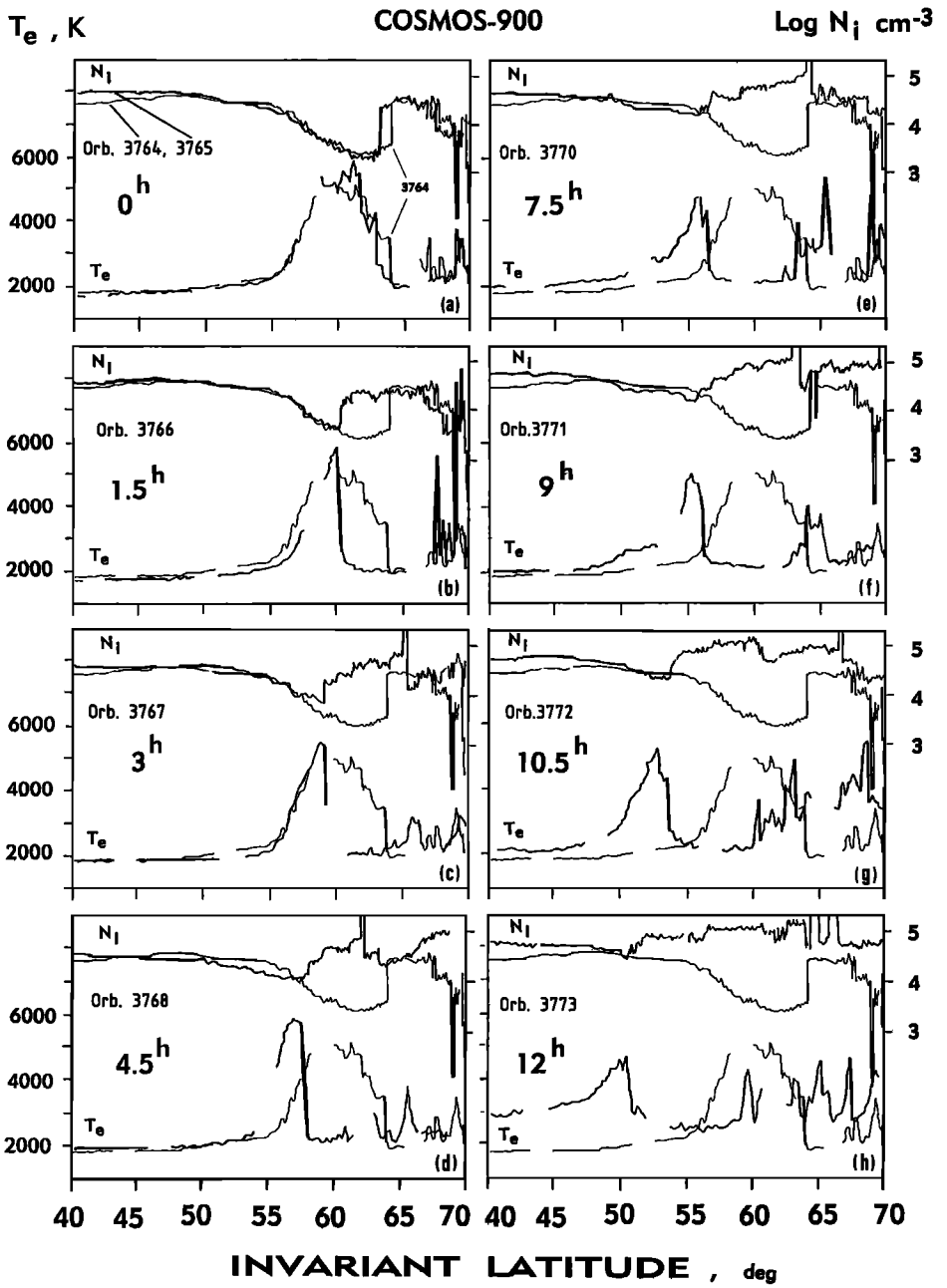

Figure 6. Illustration of the evolution of the ion density and electron temperature profiles versus L, before and during the main phase of the geomagnetic storm of December 1–2, 1977. The high spatial resolution (12 km of the ion measurements and 36 km of the electron temperature measurements) helped to determine (for the first time in 1977) the extreme steepness of these density and temperature profiles. The equatorward shift of the auroral ionization is shown. The associated erosion of the poleward wing of the SETE (and of the corresponding high-altitude plasmasphere) are also evidenced in this unique series of observations. The orbital period of Cosmos 900 is 1.5 hours. This governs the time recurrence of each set of observations. In each of the eight panels the density and temperature profiles corresponding to the prestorm orbit (3764) have been given for comparison. Note that it takes 3–4 hours after the beginning of the geomagnetic storm before the ionization front and the steepened poleward ledge of the SETE has moved to invariant latitudes lower than that of the peak temperature of the prestorm SETE.

More general and structured dynamical electric field models of the magnetosphere taking into account this effect are required in the future to interpret high-resolution observations like illustrated in Figure 6 [see also *Carpenter*, 1995]. Indeed, important effects have been included in earlier quasi-static and time-dependent magnetospheric convection electric fields, for example, (1) large induced electric fields which, recently, have been shown to be of paramount importance during geomagnetic storm [*Li et al.*, 1993, 1994; *Hudson et al.*, 1995] and (2) finite gyroradius effects resulting from the different mass and momentum of electrons and ions (J. F. Lemaire et al., unpublished manuscript, 1996). The latter effects are ignored in

MHD models as well as in kinetic models based on the guiding center approximation. This leads to the general conclusion that space weather models of the magnetosphere cannot exclusively be built on a global/large-scale magnetospheric convection flow pattern. As in meteorology, they will have to take into account the existence and the effects of sharp "fronts" separating cold and hot air masses or plasma volumes in the magnetosphere.

Present-day magnetospheric convection models are unable to explain the observations reported in Figure 6, that is, the sharpness of the plasma density wall, the sharpness of the poleward edge of the SETE, and the time evolution of its erosion during the geomagnetic storm of December 1, 1977.

4.2. Interface Between Hot and Colder Plasma Clouds

The ionization wall at the equatorward edge of the auroral region is considered to be the projection of the inner edge of the plasma sheet. We propose that it corresponds to the field-aligned projection of a sharp surface separating, on one side, hot plasma of the plasma sheet, and on the other side, the colder plasma in the plasmatrough or plasmapause region. This interpretation is supported by a quantitative kinetic model recently developed by J. F. Lemaire et al. (unpublished manuscript, 1996).

4.3. Asymmetric Erosion of SETE

The widths of the SETE wings on both sides of the T_e maximum are indicated by vertical lines in Figure 5b. It can be seen that during quiet geomagnetic conditions (prestorm) the SETE extends in a symmetrical way on both sides.

Furthermore, during the first 3–4 hours corresponding to orbits 3765–3766, Figure 5b indicates that the low-latitude wing of the SETE remains unperturbed, while the poleward wing is rapidly eroded. There is no additional heat deposition equatorward of the SETE maximum during this initial phase. It is only 3–4 hours after the storm commencement that this part of the midlatitude ionosphere is gradually heated. The ionospheric temperature at $\Lambda = 40°–45°$ remains unchanged for almost 10 hours. The first indication of a temperature increase is seen in Figure 6g (at $t = 10.5$ hours). Twelve hours after the storm commencement the maximum peak temperature has moved down to $\Lambda = 51°$ ($L = 2.5$), but the width of the propagating temperature enhancement has remained approximately constant (see Figure 5b and Figure 6d–6h).

4.4. Association Between N_i and T_e Ledges

The peaks in electron temperature are known to coincide with SAR arcs when the latter are observable. They are considered to be caused by plasmaspheric electron heated by Coulomb collisions with ring current protons [*Cole*, 1965] and O^+ ions [*Kozyra et al.*, 1987]. *Cornwall et al.* [1971] proposed Landau damping of ions cyclotron waves as an alternate way of heating the cold plasmaspheric electrons (<1 eV). These heating mechanisms take place in the plasmapause region where cold plasma is overlapping with the ring current region. In all cases the electron heat is conducted from the high-altitude plasmapause region into the underlying F region, where particles forming the tail of the electron velocity distribution excite the $O(^1D)$ state of neutral atomic oxygen. Later deexcitation of the oxygen atoms produces the emission at 630 nm that is observed as a red arc (SAR arc) observed from ground.

Kozyra et al. [1987] found also that rather symmetric profiles of T_e associate with SAR arcs, which are generally observed during the storm recovery phase, are consistent with the equatorial density profiles of ring current O^+ ions of energies of 10–20 keV. However, no explanation has yet been proposed for the steep temperature gradient formed during the initial and main phase of a magnetic storm on the poleward wing of SETE. By now all of what the sequence of N_i and T_e profiles of Figure 6 are able to tell us is that the sharp ionospheric temperature gradient is closely associated with the propagating auroral ionization wall during the main phase of the storm. This association between N_i and T_e ledges is not yet understood and needs more investigations. This issue is beyond the grasp of this paper, and our observations, of course, are unable to resolve this question.

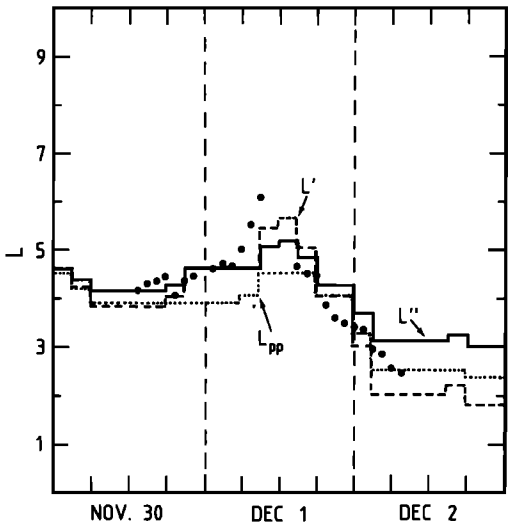

Figure 7. Values of L', the location of the SETE peak temperature in the nightside versus universal time as predicted by the relation (2) determined by *Brace et al.* [1988] from DE 2 Langmuir probe electron temperature measurements ($T_{e,\mathrm{cold}}$) for solar maximum conditions. The modified Kp' index giving the highest Kp value during the 12-hour period preceding the measurements, has been used to determine L' and L'' given by (3) for solar minimum conditions from AE-C observations. The equatorial plasmapause positions (L_{pp}) predicted by (1) determined by *Carpenter and Park* [1973] from whistler observations are also shown for the period corresponding to the December 1–2 geomagnetic storm. The solid dots give the L values corresponding to the SETE peak temperature as measured by Cosmos 900 during this period of time.

4.5. Variation of the Electron Temperature Peak With Magnetic Activity

The upper solid lines in Figure 5c show the value of the peak temperature measured by Cosmos 900 before and during the storm. These peak values vary between 3000 and 6000 K. From DE 2 observations in the altitude range 350–600 km, *Kozyra et al.* [1986] found a linear variation of the nightside $T_{e,\max}$ as a function of Kp'

$$T_{e,\max} = 1570 + 318\ Kp' \qquad (4)$$

The predictions of this linear fit are shown by the dotted line in Figure 5c. It can be seen that the maximum temperature values predicted by this relation (dotted line) are much lower than those measured by Cosmos 900 in 1977 (upper solid lines). This difference may be accounted for by the large scatter of DE 2 data around the statistical relation (4) (see Figure 8 of *Kozyra*

et al. [1986]), but it is more likely due to the different methods used to determine the electron temperature, respectively, from Cosmos 900 and DE 2 measurements.

Indeed, from the DE 2 Langmuir probe measurements a temperature, $T_{e,\text{cold}}$, for the cold Maxwellian ionospheric electrons was deduced; indeed, these cold electrons contribute to most of the total flux measured by Langmuir probes. On the contrary, the electron temperature obtained from the Cosmos 900 measurements were determined by the slope of the current-voltage characteristics (I–V curves) averaged over an electric potential interval $\Delta V \cong kT_e/e$, which is centered around the floating potential of the probe. The electrons were assumed to have a Maxwellian velocity distribution function. However, if the electrons have a non-Maxwellian velocity distribution (e.g., Lorentzian velocity distribution) with a population of suprathermal electron forming an extended tail, the values of the effective electron temperature ($T_{e,\text{eff}}$) deduced from the slope of the current voltage characteristic are systematically larger than $T_{e,\text{cold}}$ obtained from Langmuir probe flux measurements.

Direct comparison of RF probe measurements and spherical Langmuir probe measurements of electron energy spectra have been compared by *Afonin et al.* [1975] using Cosmos 378 data between 240 and 1750 km altitude. The presence of non-Maxwellian electron velocity distributions may explain that the peak temperature values ($T_{e,\text{eff}}$) shown in Figure 5c are significantly higher than the values of $T_{e,\text{cold}}$ predicted by (4), which was deduced from DE 2 Langmuir probe average electron temperature measurements.

Since the definitions of $T_{e,\text{cold}}$ and $T_{e,\text{eff}}$ are different for the reasons indicated above, they cannot be directly compared to each other, and their variation need not necessarily follow the same trend during geomagnetic storms, as indeed shown in Figure 5c.

Kozyra et al. [1986] deduced from their statistical study of SETE that the magnitude of the electron temperature peak $T_{e,\text{max}}$ increases with increasing value of the *Dst* magnetic activity index. For altitudes below 600 km on the nightside they found

$$T_{e,\text{max}} = 2513 - 8\,Dst \qquad (5)$$

Similar results were obtained by *Büchner et al.* [1983] from Intercosmos 18 Langmuir-probe observations. The Cosmos 900 results shown in Figure 5c do not support this statistical prediction well (not shown). The lack of agreement may be due to (1) the large scatter of DE 2 (as shown in Figure 9 of *Kozyra et al.* [1986]) and (2) the different method used to determine the electron temperatures from DE 2 and Cosmos 900 data, respectively.

4.6. Electron Temperature on the Poleward Side of SETE

The ionospheric electron temperature on the polar side of the SETE is shown by the lower solid line of Figure 5c. This background temperature on the poleward side does not change during the storm, except after orbit 3770 (after 2400 UT on December 1, 1977), that is, well within the main phase of the geomagnetic storm. This implies that nearly no energy is transfered from the ring current particles except in the plasmapause region where the distribution of ring current particles overlaps with the cold plasmaspheric electrons.

4.7. Electron Temperature on the Equatorside of SETE

Figure 5d shows the change of the electron temperature in the postmidnight sector at low latitudes: at $L = 1.5$ (dashed line) and at $L = 2.0$ (solid line). Note the reduced temperature scale compared to Figure 5c. It can be seen that the low-latitude temperatures do not exceed 3000 K, even during the main phase of the geomagnetic storm.

Acknowledgments. One of the authors (J.F.L.) thanks the Belgian Institute for Space Aeronomy and the Services Fédéraux des Affaires Scientifiques, Techniques et Culturelles, who are supporting the collaboration between IKI and IASB. It is in the framework of this collaboration that this paper has been prepared based on data collected by Russian satellites more than 15 years ago.

The Editor thanks P. M. E. Décréau and two other referees for their assistance in evaluating this paper.

References

Afonin, V. V., G. L. Gdalevich, K. I. Gringauz, J. Kainarova, and J. Smilauer, Ionospheric studies conducted by the satellite Intercosmos-2, III, Ionospheric electron temperature measurements by high-frequency probe method, *Cosmic Res.*, *11*, 254–264, 1973.

Afonin, V. V., G. L. Gdalevich, and S. M. Sheronova, Ionospheric study with Cosmos-378 satellite, *Geomagn. Aeronom.*, *15*(N4), 615–620, 1975.

Aono, Y., K. Hirao, and S. Miyazaki, Positive ion density, electron density and electron temperature by Kappa-8-5 and 6 rockets, *J. Radio Res. Lab.*, *8*, 453–465, 1961.

Brace, L. H., Solar cycle variations in *F* region Te in the vicinity of the midlatitude trough based on AE-C measurements at solar maximum, *Adv. Space Res.*, *10*(11), 83–88, 1990.

Brace, L. H., and B. M. Reddy, Early electrostatic probe results from Explorer-22, *J. Geophys. Res.*, *70*, 5783–5792, 1965.

Brace, L. H., and R. F. Theis, The behavior of the plasmapause at midlatitudes: ISIS 1 Langmuir probe measurements, *J. Geophys. Res.*, *79*, 1871–1884, 1974.

Brace, L. H., B. M. Reddy, and H. G. Mayr, Global behavior of the ionosphere at 1000 kilometer altitude, *J. Geophys. Res.*, *72*, 265–283, 1967.

Brace, L. H., E. J. Maier, J. H. Hoffman, J. Whitteker, and G. G. Shepperd, Deformation of the nightside plasmasphere and ionosphere during the August 1972 geomagnetic storm, *J. Geophys. Res.*, *79*, 5211–5218, 1974.

Brace, L. H., C. R. Chappell, M. O. Chandler, R. H. Comfort, J. L. Horwitz, and W. R. Hoegy, *F* region electron temperature signatures of the plasmapause based on dynamics Explorer 1 and 2 measurements, *J. Geophys. Res.*, *93*, 1896–1908, 1988.

Büchner, J., H. R. Lehmann, and J. Rendtel, Properties of subauroral electron temperature peak observed by Langmuir-probe measurements on board Intercosmos-18, *Gerlands Beitr. Geophys.*, *92*, 368–373, 1983.

Carpenter, D. L., Whistler studies of the plasmapause in the magnetosphere, 1, Temporal variations in the position of the knee and some evidence on plasma motions near the knee, *J. Geophys. Res.*, *71*, 693–709, 1966.

Carpenter, D. L., Whistler evidence of the dynamic behavior of the duskside bulge in the plasmasphere, *J. Geophys. Res.*, *75*, 3837–3847, 1970.

Carpenter, D. L., Earth's plasmasphere awaits rediscovery, *Eos. Trans. AGU*, *76*(9), 89–92, 1995.

Carpenter, D. L., and R. R. Anderson, An ISEE/whistler model of equatorial electron density in the magnetosphere, *J. Geophys. Res.*, *97*, 1097–1108, 1992.

Carpenter, D. L., and C. G. Park, On what ionosphere workers should know about the plasmapause-plasmasphere, *Rev. Geophys.*, *11*, 133–154, 1973.

Carpenter, D. L., B. L. Giles, C. R. Chappell, P. M. E. Decreau, R. R. Anderson, A. M. Persoon, A. J. Smith, Y. Corcuff, and P. Canu, Plasmasphere dynamics in the duskside bulge region: A new look at an old topic, *J. Geophys. Res.*, *98*, 19,243–19,271, 1993.

Chappell, C. R., K. K. Harris, and G. W. Sharp, A study of the influence of magnetic activity on the location of the plasmapause as measured by Ogo 5, *J. Geophys. Res.*, *75*, 50–56, 1970.

Chappell, C. R., K. K. Harris, and G. W. Sharp, The dayside of the plasmasphere, *J. Geophys. Res.*, *76*, 7632–7647, 1971.

Cole, K. D., Stable auroral red arcs, sinks for energy of *Dst* main phase, *J. Geophys. Res.*, *70*, 1689–1706, 1965.

Cornwall, J. M., F. V. Coroniti, and R. M. Thorne, Unified theory of SAR arc formation at the plasmapause, *J. Geophys. Res.*, *76*, 4428–4435, 1971.

Foster, J. C., C. G. Park, L. Brace, J. R. Burrows, J. H. Hoffman, E. J. Maier, and J. H. Whitteker, Plasmapause signatures in the ionosphere and magnetosphere, *J. Geophys. Res.*, *83*, 1175–1182, 1978.

Grebowsky, J., N. Maynard, Y. Tulunay, and L. Lanzerotti, Coincident observations of ionospheric troughs and the equatorial plasmapause, *Planet. Space Sci.*, *24*, 1177–1185, 1976.

Green, J. L., J. H. Waite Jr., C. R. Chappell, M. O. Chandler, J. R. Doupnik, P. G. Richards, R. Heelis, S. D. Shawhan, and L. H. Brace, Observations of ionospheric magnetospheric coupling: DE and Chatanika coincidences, *J. Geophys. Res.*, *91*, 5803–5815, 1986.

Gringauz, K. I., The structure of the Earth's ionized gas envelope based on local charged particle concentrations measured in USSR, *Adv. Space Res.*, *II*, 574–592, 1961.

Gringauz, K. I., Plasmasphere and its interaction with the ring current, *Space Sci. Rev.*, *34*, 245–257, 1983.

Gringauz, K. I., and V. V. Bezrukikh, Asymmetry of the Earth's plasmasphere in the direction noon-midnight from Prognoz-1 and Prognoz-2 data, *J. Atmos. Terr. Phys.*, *38*, 1071–1076, 1976.

Gringauz, K. I., V. V. Bezrukikh, and V. V. Afonin, The plasmasphere physics problems in the light of the measurements from Prognoz-5, in *All-Union Conference on the Results of IMS-Project*, Turk. Acad. of Sci., Ashabad, p. 17, 1981.

Horwitz, J. L., L. H. Brace, R. H. Comfort, and C. R. Chappell, Dual-spacecraft measurements of plasmasphere-ionosphere coupling, *J. Geophys. Res.*, *91*, 11,203–11,216, 1986.

Hudson, M. K., A. D. Kotelnikov, X. Li, I. Roth, M. Temerin, J. Wygant, J. B. Blake, and M. S. Gussenhoven, Simulation of proton radiation belt formation during the March 24, 1991 SSC, *Geophys. Res. Lett.*, *22*, 291–294, 1995.

Kozyra, J. U., L. H. Brace, T. E. Cravens, and A. F. Nagy, A statistical study of the subauroral electron temperature enhancement using Dynamics Explorer 2 Langmuir probe observations, *J. Geophys. Res.*, *91*, 11,270–11,280, 1986.

Kozyra, J. U., E. G. Shelley, R. H. Comfort, L. H. Brace, T. E. Cravens, and A. F. Nagy, The role of ring current O^+ in the formation of stable auroral red arcs, *J. Geophys. Res.*, *92*, 7487–7502, 1987.

Lemaire, J., and R. W. Schunk, Plasmaspheric convection with non-closed streamlines, *J. Atmos. Terr. Phys.*, *56*, 1629–1633, 1994.

Li, X., I. Roth, M. Temerin, J. R. Wygant, M. K. Hudson, and J. B. Blake, Simulation of the prompt energization and transport of radiation belt particules during the March 24, 1991 SSC, *Geophys. Res. Lett.*, *20*, 2423–2426, 1993.

Li, X., M. K. Hudson, J. B. Blake, I. Roth, M. Temerin, and J. R. Wygant, Observation and simulation of the rapid formation of a new electron radiation belt during March 24, 1991 SSC, paper presented at Workshop on Earth's Trapped Particle Environment, Taos, N. M. Aug. 14–19, 1995.

Miller, N. J., L. H. Brace, N. W. Spencer, and G. R. Carignan, DE 2 observations of disturbances in the upper atmosphere during a geomagnetic storm, *J. Geophys. Res.*, *95*, 21,017–21,031, 1990.

Muldrew, D. B., *F* layer ionization troughs deduced from Alouette data, *J. Geophys. Res.*, *70*, 2635–2650, 1965.

Peyrimat, C., and D. Fontaine, Numerical simulation of magnetospheric convection including the effect of field-aligned currents and electron precipitation, *J. Geophys. Res.*, *90*, 11,155–11,176, 1994.

Pierrard, V., and J. Lemaire, Lorentzian model ion-exosphere, *J. Geophys. Res.*, *101*, 7923–7934, 1996.

Raitt, W. J., The temporal and spatial development of midlatitude thermospheric electron temperature enhancements during a geomagnetic storm, *J. Geophys. Res.*, *79*, 4703–4708, 1974.

Rycroft, M. J., and S. J. Burnell, Statistical analysis of movements of the ionospheric trough and the plasmapause, *J. Geophys. Res.*, *75*, 5600–5604, 1970.

Rycroft, M. J., and J. O. Thomas, The magnetospheric plasmapause and the electron density trough at the Alouette-1 orbit, *Planet. Space Sci.*, *18*, 65–80, 1970.

Stern, D. P., Large-scale electric fields in the Earth's magnetosphere, *Rev. Geophys.*, *15*, 156–194, 1977.

Taylor, H. A., H. C. Brinton, and A. R. Deshmukh, Observations of irregular structure in thermal ion distributions in the duskside magnetosphere, *J. Geophys. Res.*, *75*, 2481–2489, 1970.

Thomas, J. O., and M. K. Andrews, Transpolar exospheric plasma, 1, Plasmasphere termination, *J. Geophys. Res.*, *73*, 7407–7417, 1968.

Titheridge, J. E., Plasmapause effects in the topside ionosphere, *J. Geophys. Res.*, *81*, 3227–3233, 1976.

Tulunay, Y., and J. Sayers, Characteristics of the mid-latitude trough as determined by the electron density experiment on Ariel III, *J. Atmos. Terr. Phys.*, *33*, 1737–1761, 1971.

Volland, H., A semi-empirical model of large-scale magnetospheric electric fields, *J. Geophys. Res.*, *78*, 171–180, 1973.

Volland, H., Models of global electric fields within the magnetosphere, *Ann. Geophys.*, *31*, 159–173, 1975.

Volland, H., A model of the magnetospheric electric convection field, *J. Geophys. Res.*, *83*, 2695–2699, 1978.

V. V. Afonin and V. S. Bassolo, Space Research Institute, Profsoyusnaya 84/32, Moscow, Russia.

J. F. Lemaire, Institut d'Aéronomie Spatiale de Belgique, 3 Avenue Circulaire, Bruxelles, B-1080, Belgium. (e-mail: jl@plasma.oma.be)

J. Smilauer, Institute of Atmospheric Physicis, Bocni II, 14131 Prague, Czech Republic.

(Received June 5, 1995; revised August 9, 1996;
accepted August 12, 1996.)